AN IRIS RECOGNITION SYSTEM USING PHASE-BASED IMAGE MATCHING

Kazuyuki Miyazawa, Koichi Ito, Takafumi Aoki

Graduate School of Information Sciences, Tohoku University,
Sendai 980–8579, Japan
∗E-mail: miyazawa@aoki.ecei.tohoku.ac.jp

Koji Kobayashi, Atsushi Katsumata

Yamatake Corporation,
Higashi-shinagawa 140-0002, Japan

ABSTRACT

This paper presents an implementation of iris recognition algorithm using phase-based image matching — an image matching technique using phase components in 2D Discrete Fourier Transforms (DFTs) of given images. Our experimental observation clearly shows that the use of phase components of iris images makes possible to achieve highly accurate iris recognition even for low-quality iris images. In this paper, we consider the problem of designing a compact phase-based iris recognition algorithm especially suitable for hardware implementation. We also present prototype implementation of an iris recognition system based on the proposed algorithm. The prototype system fully utilizes state-of-the-art DSP (Digital Signal Processor) technology to achieve real-time iris recognition capability within a compact hardware module.

Index Terms— Identification of persons, image matching, image processing

1. INTRODUCTION

Biometric authentication has been receiving extensive attention over the past decade with increasing demands in automated personal identification. Among many biometrics techniques, iris recognition has gained match attention due to its high reliability for personal identification [1]–[3].

A major approach for iris recognition today is to generate feature vectors from individual iris images and to perform iris matching based on some distance metrics [1], [2]. Most of the commercial iris recognition systems implement a famous algorithm using *iriscodes* proposed by Daugman [1]. One of the difficult problems in feature-based iris recognition is that the matching performance is significantly influenced by many parameters in feature extraction process (e.g., spatial position, orientation, center frequencies and size parameters for 2D Gabor filter kernel), which may vary depending on environmental factors of iris image acquisition.

Addressing the problem, we have proposed an efficient iris recognition algorithm [4], [5] using phase-based image matching — an image matching technique using phase components in 2D Discrete Fourier Transforms (DFTs) of given images. The proposed algorithm achieves very low error rate (EER=0.0032%) for CASIA iris image database [6]. In this paper, we discuss modification of the proposed algorithm dedicated to compact hardware implementation and evaluate its impact on recognition performance and computation time.

We also present prototype implementation of an iris recognition system based on the modified algorithm. Note that conventional iris recognition devices are large and expensive in general. The prototype utilizes state-of-the-art DSP (Digital Signal Processor) technology to achieve real-time recognition capability within a compact hardware module of size 15cm×10cm×3.5cm (HWD). The result suggests a possibility of DSP-based biometrics technology particularly suitable for mobile applications.

2. PHASE-BASED IRIS RECOGNITION ALGORITHMS

This section describes possible modification of the phase-based iris recognition algorithm [4], [5] dedicated to compact hardware implementation. Figure 1 (a) shows the baseline algorithm for iris recognition, which consists of a preprocessing stage and a matching stage. We briefly overview these stages.

2.1. Preprocessing

An iris image contains some irrelevant parts (e.g., eyelid, sclera, pupil, etc.). Also, the size of an iris may vary depending on camera-to-eye distance and lighting condition. Therefore, the original image needs to be normalized.

(i) Iris Localization: This step is to detect the inner (iris/pupil) boundary and the outer (iris/sclera) boundary in the original image. We model the inner boundary as an ellipse, and the outer boundary as a circle.

(ii) Iris Normalization: Next step is to normalize iris images to compensate for iris deformation. In order to avoid eyelashes, we use only lower half portion of the iris (Figure 1 (b)) and unwrap the region to a rectangular block of a fixed size (128×256 pixels) as illustrated in Figure 1 (c). The eyelid region is then masked as in Figure 1 (d).

2.2. Matching

The key idea of the proposed algorithm is to use phase-based image matching for image alignment and matching score calculation (see Figure 1 (a)). Before discussing the algorithm,

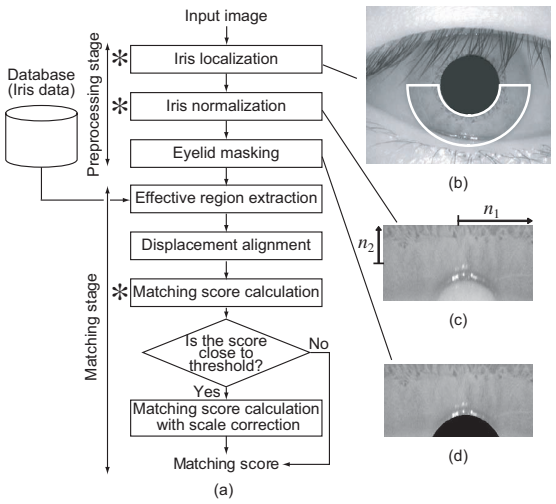

Fig. 1. Baseline algorithm: (a) flow diagram, (b) original image, (c) normalized image (n_1 axis corresponds to the angle of polar coordinate system and n_2 axis corresponds to the radius), and (d) normalized image with eyelid masking.

we introduce the principle of phase-based image matching using the Phase-Only Correlation (POC) function.

Consider two $N_1 \times N_2$-pixel images, $f(n_1, n_2)$ and $g(n_1, n_2)$, where we assume that the index ranges are $n_1 = -M_1, \cdots, M_1$ ($M_1 > 0$) and $n_2 = -M_2, \cdots, M_2$ ($M_2 > 0$) for mathematical simplicity, and hence $N_1 = 2M_1 + 1$ and $N_2 = 2M_2 + 1$. Let $F(k_1, k_2)$ and $G(k_1, k_2)$ denote the 2D DFTs of the two images. The cross-phase spectrum $R_{FG}(k_1, k_2)$ is given by

$$R_{FG}(k_1, k_2) = \frac{F(k_1, k_2)\overline{G(k_1, k_2)}}{|F(k_1, k_2)\overline{G(k_1, k_2)}|} = e^{j\theta(k_1, k_2)}, \qquad (1)$$

where $k_1 = -M_1, \cdots, M_1$, $k_2 = -M_2, \cdots, M_2$, $\overline{G(k_1, k_2)}$ is the complex conjugate of $G(k_1, k_2)$ and $\theta(k_1, k_2)$ denotes the phase difference of $F(k_1, k_2)$ and $G(k_1, k_2)$. The POC function $r_{fg}(n_1, n_2)$ is the 2D Inverse DFT of $R_{FG}(k_1, k_2)$.

When two images are similar, their POC function gives a distinct sharp peak. When they are not similar, the peak drops significantly. The height of the peak gives a good similarity measure for image matching, and the location of the peak shows the translational displacement between the images.

Our observation shows that the 2D DFT of a normalized iris image contains meaningless phase components in high frequency domain, and that the effective frequency band of the normalized iris image is wider in k_1 direction than in k_2 direction (see Figure 2). To evaluate the similarity using the inherent frequency band within iris textures, we employ BLPOC (Band-Limited Phase-Only Correlation) function.

Assume that the ranges of the significant frequency band are $k_1 = -K_1, \cdots, K_1$ ($0 \leq K_1 \leq M_1$) and $k_2 = -K_2, \cdots, K_2$ ($0 \leq K_2 \leq M_2$), where as shown in Figure 2 (b). Thus, the effective size of frequency spectrum is given by $L_1 = 2K_1 + 1$ and $L_2 = 2K_2 + 1$. The BLPOC function is given by

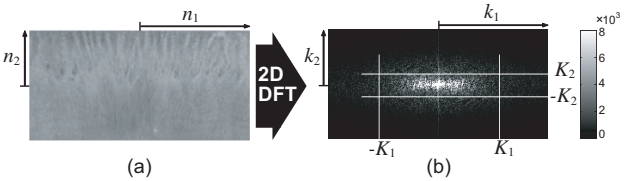

Fig. 2. Normalized iris image in (a) spatial domain, and in (b) frequency domain (amplitude spectrum), where $K_1 = 0.55M_1$ and $K_2 = 0.2M_2$.

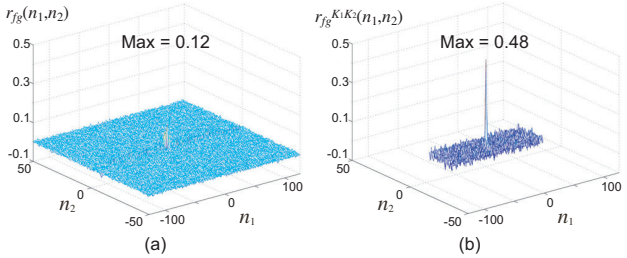

Fig. 3. Example of genuine matching using the original POC function and the BLPOC function: (a) original POC function $r_{fg}(n_1, n_2)$, and (b) BLPOC function $r_{fg}^{K_1K_2}(n_1, n_2)$.

$$r_{fg}^{K_1K_2}(n_1, n_2) = \frac{1}{L_1 L_2} \sum_{k_1, k_2} R_{FG}(k_1, k_2) W_{L_1}^{-k_1 n_1} W_{L_2}^{-k_2 n_2}, \qquad (2)$$

where $n_1 = -K_1, \cdots, K_1$, $n_2 = -K_2, \cdots, K_2$, $W_{L_1} = e^{-j\frac{2\pi}{L_1}}$, $W_{L_2} = e^{-j\frac{2\pi}{L_2}}$ and $\sum_{k_1, k_2}$ denotes $\sum_{k_1=-K_1}^{K_1} \sum_{k_2=-K_2}^{K_2}$.

Figure 3 shows an example of genuine matching using the original POC function and the BLPOC function. The BLPOC function provides better discrimination capability than that of the original POC function. In the following, we describe the detailed process of the matching stage (shown in Figure 1 (a)) using the BLPOC function.

(i) Effective region extraction: Given a pair of normalized iris images $\tilde{f}(n_1, n_2)$ and $\tilde{g}(n_1, n_2)$ to be compared, the purpose of this process is to extract the effective regions $f(n_1, n_2)$ and $g(n_1, n_2)$ of the same size as illustrated in Figure 4 (a). When the extracted region becomes too small to perform image matching, we extract multiple effective sub-regions from each iris image by changing the width parameter w (Figure 4 (b)). In our experiments, we extract 6 sub-regions from an iris image by changing the parameter w as 55, 75 and 95 pixels.

(ii) Displacement alignment: This step is to align the translational displacement between the extracted regions. The displacement parameters can be obtained from the peak location of the BLPOC function $r_{fg}^{K_1K_2}(n_1, n_2)$.

(iii) Matching score calculation: We calculate the BLPOC function between the aligned images and evaluate the matching score as the maximum correlation peak value. When multiple sub-regions are extracted as illustrated in Figure 4 (b), the matching score is calculated by taking an average for effective sub-regions. If the matching score is close to threshold value to separate genuines and impostors, we calculate the matching score with scale correction.

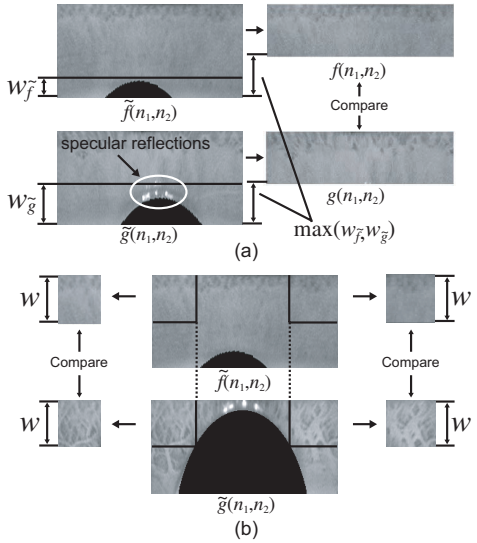

Fig. 4. Effective region extraction: (a) normal case, and (b) case when multiple sub-regions should be extracted.

2.3. Simplified Algorithm

For typical embedded systems, the overall iris recognition algorithm should be implemented within a single DSP or an MPU (Micro Processing Unit), which imposes severe limitations on available computation power. Hence, we consider here a simplified version of the original algorithm, where only the marked "$*$" three steps in Figure 1 (a) are adopted, while omitting other four steps. An important advantage of the simplified algorithm is that we do not need to register the iris "image" data directly in the system. In practice, only the Fourier phase components are to be stored in the system.

3. EXPERIMENTAL EVALUATION

This section describes a set of experiments using CASIA iris image database [6] for evaluating the proposed algorithm. This database contains 756 eye images (108 eyes and 7 images of each eye). We evaluate the genuine matching scores and the impostor matching scores for all the possible combinations (genuine: 2,268 attempts, impostor: 283,122 attempts). We compare the original algorithm and the simplified algorithm. Figure 5 shows the ROC (Receiver Operating Characteristic) curves for the algorithms. The ROC curve illustrates FNMR (False Non-Match Rate) against FMR (False Match Rate) at different thresholds on the matching score. EER (Equal Error Rate) shown in the figure is the error rate where FNMR and FMR are equal. As observed in the figure, the original algorithm shows very low EER (0.0032%), which is one of the best records reported on the database. The performance penalty due to the simplification is about 8% increase in EER.

Our observation shows that this performance degradation is mainly caused by the elimination of the eyelid masking and the effective region extraction steps. Note that CASIA iris image database contains many iris images whose irises are

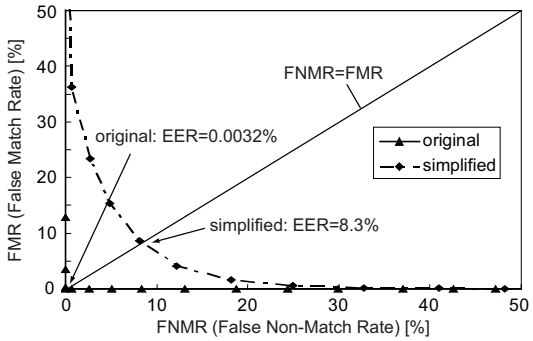

Fig. 5. ROC curves and EERs.

heavily occluded by eyelids. Thus, the eyelid masking and the effective region extraction steps have a significant impact on the performance. In a practical system, however, such a difficult condition does not happen so often. On the other hand, the processing time could be greatly reduced by the simplification (omitting four steps in Figure 1 (a)), which allows the system to perform multiple matching within a short time. This leads to better GAR (Genuine Accept Rate) for users.

4. IRIS RECOGNITION SYSTEM

We have already developed commercial fingerprint verification units using phase-based image matching [7]–[10]. The goal of this paper is to demonstrate that the same approach is also effective for designing iris recognition devices. Note that conventional iris recognition devices are large and expensive in general. We can implement a compact DSP-based iris recognition system using the simplified algorithm described in the previous section. Figure 6 (a) shows the developed iris recognition device of size 15cm$\times$10cm$\times$3.5cm (HWD).

4.1. System Architecture

Figure 6 (b) shows the block diagram of the device, which consists of two PWBs (Printed Wiring Boards), camera PWB and DSP PWB. The camera PWB contains a pair of cameras with surrounding infrared LEDs for lighting, and a full-color LED for status indication. Camera resolution is 1320$\times$1024 pixels and only 640$\times$480 pixels fixed area is used for image processing. An infrared band-pass filter is attached to each camera to capture infrared iris images.

The DSP PWB contains a DSP, a Flash ROM, two dynamic and one static RAM chips, a codec for voice message, and a serial communication port. The DSP is well suited for 2D DFT computation required for phase-based image matching. In our system, a fixed-point DSP is used because it runs at higher clock frequency with lower power consumption compared with floating-point DSPs.

4.2. Procedure of Iris Recognition

For capturing good-quality iris images, the device has mechanisms of a rotatable camera head, a mirror for face position-

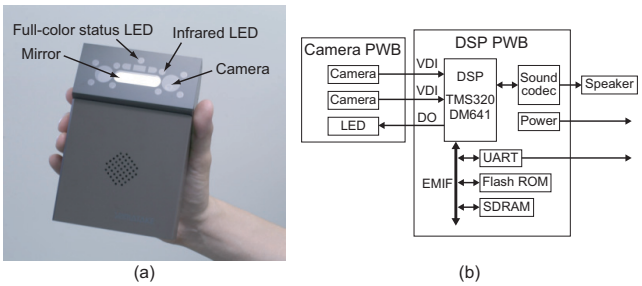

Fig. 6. Iris recognition system: (a) prototype of the device, and (b) block diagram.

ing, and an LED status indicator. The status LED changes its color depending on camera-to-eye distance. Figure 7 (a) shows the operation flowchart for the iris recognition device, which consists of (i) the image capture stage and (ii) the iris recognition stage. We adopt the simplified algorithm described in the Section 2.3 for the iris recognition stage.

The purpose of the image capture stage, on the other hand, is to capture iris images at the specified distance ($\sim$10cm in our prototype system). To do this, the system estimates the camera-to-eye distance from corneal reflection patterns of infrared LEDs. Figure 7 (b) shows an example of captured iris image, where corneal reflections of four infrared LEDs are observed. First, the system detects the four-point reflections by using a 41×41 spatial filter shown in Figure 7 (c). The filtered image is shown in Figure 7 (d). If there exists a clear four-point reflection pattern, the filter outputs a sharp peak at the center of the pattern. After detecting the four-point pattern, the system can estimate the camera-to-eye distance using the size of the pattern. Only when the size is in an appropriate range, the captured image is used for recognition.

In our prototype, the overall iris recognition procedure (Figure 7 (a)) takes only 1 second on the state-of-the-art DSP (Texas Instruments TMS320DM641 400MHz), which clearly demonstrates a potential possibility of DSP-based iris recognition applicable to a wide range of embedded applications.

5. CONCLUSION

The authors have already developed actual fingerprint verification units using phase-based image matching [7]–[10]. In this paper, we have demonstrated that the same approach is also effective for iris recognition. It can also be suggested that the proposed approach will be useful for multimodal biometric system having iris and fingerprint recognition capabilities.

The correlation filter based biometrics described in [3] is closely related to our approach and suggests important ideas for reducing the computational complexity. Detailed investigations are being left for future study.

Acknowledgment Portions of the research in this paper use CASIA iris image database collected by Institute of Automation, Chinese Academy of Sciences.

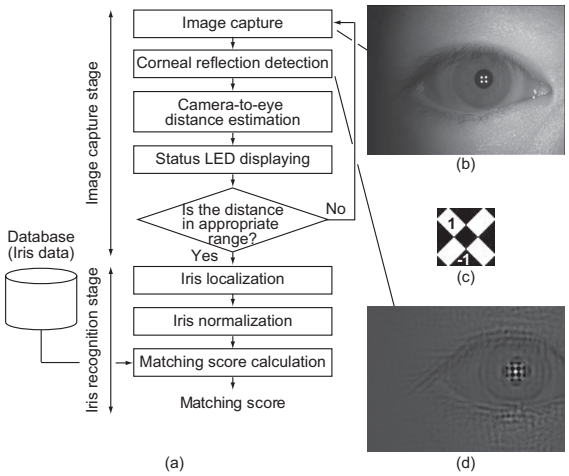

Fig. 7. Procedure of iris recognition: (a) overall procedures, (b) example of captured iris image, (c) filter for reflection detection, and (d) filtered image.

6. REFERENCES

[1] J. Daugman, "High confidence visual recognition of persons by a test of statistical independence," *IEEE Trans. Pattern Analy. Machine Intell.*, vol. 15, no. 11, pp. 1148–1161, Nov. 1993.

[2] L. Ma, T. Tan, Y. Wang, and D. Zhang, "Efficient iris recognition by characterizing key local variations," *IEEE Trans. Image Processing*, vol. 13, no. 6, pp. 739–750, June 2004.

[3] B. Kumar, C. Xie, and J. Thornton, "Iris verification using correlation filters," *Proc. 4th Int. Conf. Audio- and Video-based Biometric Person Authentication*, pp. 697–705, 2003.

[4] K. Miyazawa, K. Ito, T. Aoki, K. Kobayashi, and H. Nakajima, "An efficient iris recognition algorithm using phase-based image matching," *Proc. Int. Conf. on Image Processing*, pp. II–49–II–52, Sept. 2005.

[5] K. Miyazawa, K. Ito, T. Aoki, K. Kobayashi, and H. Nakajima, "A phase-based iris recognition algorithm," *Lecture Notes in Computer Science (ICB2006)*, vol. 3832, pp. 356–365, Jan. 2006.

[6] CASIA iris image database ver 1.0. http://www.sinobiometris.com

[7] K. Ito, H. Nakajima, K. Kobayashi, T. Aoki, and T. Higuchi, "A fingerprint matching algorithm using phase-only correlation," *IEICE Trans. Fundamentals*, vol. E87-A, no. 3, pp. 682–691, Mar. 2004.

[8] K. Ito, A. Morita, T. Aoki, T. Higuchi, H. Nakajima, and K. Kobayashi, "A fingerprint recognition algorithm combining phase-based image matching and feature-based matching," *Lecture Notes in Computer Science (ICB2006)*, vol. 3832, pp. 316–325, Jan. 2006.

[9] H. Nakajima, K. Kobayashi, M. Morikawa, K. Atsushi, K. Ito, T. Aoki, and T. Higuchi, "Fast and robust fingerprint identification algorithm and its application to residential access controller," *Lecture Notes in Computer Science (ICB2006)*, vol. 3832, pp. 326–333, Jan. 2006.

[10] Products using phase-based image matching. http://www.aoki.ecei.tohoku.ac.jp/poc/